Obesity Surgery (2019) 29:2158–2165
https://doi.org/10.1007/s11695-019-03800-z

ORIGINAL CONTRIBUTIONS

Gastric Bypass Surgery Improves the Skeletal Muscle Ceramide/S1P Ratio and Upregulates the AMPK/ SIRT1/ PGC-1α Pathway in Zucker Diabetic Fatty Rats

Hazel Huang[1] · Ali Aminian[2] · Monique Hassan[2] · Olivia Dan[2] · Christopher L. Axelrod[1,3] · Philip R. Schauer[2] · Stacy A. Brethauer[2] · John P. Kirwan[1,3]

Published online: 26 February 2019

Abstract

Purpose Roux-en-Y gastric bypass (RYGB) is associated with remission of type 2 diabetes. However, the cellular and molecular mechanisms remain unknown. We hypothesized that RYGB would increase peroxisome proliferator-activated receptor gamma coactivator 1-alpha (PGC-1α), sirtuin-1 (SIRT1), AMPK/pAMPK, and citrate synthase (CS) protein expression and decrease insulin resistance and these changes would be mediated by sphingolipids, including ceramides and the sphingolipid metabolite sphingosine-1 phosphate (S1P).

Materials and Methods Male ZDF rats were randomized to RYGB ($n = 7$) or sham surgery ($n = 7$) and harvested after 28 days. Total tissue ceramide, ceramide subspecies (C14:0, C16:0, C18:0, C18:1, C20:0, C24:0, and C24:1), and S1P were quantified in the white gastrocnemius muscle using LC-ESI-MS/MS after separation with HPLC. Total SIRT1, AMPK, PGC-1α, and CS protein expression were measured by Western blot.

Results Body weight, fasting glucose, insulin, and HOMA-IR decreased significantly after RYGB compared with sham control. These changes were paralleled by lower total ceramide (483.7 ± 32.3 vs. 280.1 ± 38.8 nmol/g wwt), C18:0 ceramide subspecies ($P < 0.05$), higher S1P (0.83 ± 0.05 vs. 1.54 ± 0.21 nmol/g wwt, $P < 0.05$), and a lower ceramide/S1P ratio ($P < 0.05$) in the RYGB versus sham group. AMPK, pAMPK, SIRT1, PGC-1α, and CS protein expression was also higher after RYGB ($P < 0.05$). The ceramide/S1P ratio correlated with weight loss ($r = 0.48$, $P = 0.08$), insulin resistance ($r = 0.61$, $P = 0.02$), PGC-1α ($r = -0.51$, $P < 0.06$), CS ($r = -0.63$, $P = 0.01$), and SIRT1 ($r = -0.54$, $P < 0.04$).

Conclusion Our data demonstrate that sphingolipid balance, and increased AMPK, SIRT1, PGC-1α, and CS protein expression are part of the mechanism that contributes to the remission of diabetes after RYGB surgery.

Keywords PGC-1α · SIRT1 · AMPK · Citrate synthase · Ceramide · Sphingosine-1 phosphate · Gastric bypass · Obesity · Diabetes · Weight loss · Bariatric · Lipotoxicity

✉ John P. Kirwan
john.kirwan@pbrc.edu

Hazel Huang
huanghazel65@gmail.com

Ali Aminian
aminiaa@ccf.org

Monique Hassan
nysurg@gmail.com

Olivia Dan
dano@ccf.org

Christopher L. Axelrod
christopher.axelrod@pbrc.edu

Philip R. Schauer
schauep@ccf.org

Stacy A. Brethauer
brethas@ccf.org

[1] Department of Pathobiology, Cleveland Clinic, Lerner Research Institute, Cleveland, OH, USA

[2] Cleveland Clinic, Bariatric and Metabolic Institute, Cleveland, OH, USA

[3] Integrated Physiology and Molecular Medicine Laboratory, Pennington Biomedical Research Center, 6400 Perkins Road, L-4030, Baton Rouge, LA 70808, USA

Introduction

Bariatric surgical procedures, including Roux-en-Y gastric bypass (RYGB), biliopancreatic diversion (BPD), and vertical sleeve gastrectomy (VSG), result in a rapid and durable remission of type 2 diabetes (T2D) [1–3]. Restoration of euglycemia has been reported within days after surgical intervention, suggesting that the metabolic effects are weight loss independent [4]. However, the mechanisms driving surgical remission of T2D remain elusive.

Progression of peripheral insulin resistance and defective insulin secretion are observed in both obesity and T2D. This is most notably demonstrated by epidemiological studies identifying that approximately 90% of T2D's are overweight and/or obese [5]. Increased visceral adiposity is observed in obesity and T2D and leads to the accumulation of lipid in non-adipose tissue, such as the pancreas, skeletal muscle, kidney, and liver. This ectopic lipid accumulation can activate stress and apoptotic signaling pathways, ultimately leading to cellular dysfunction and death. Indeed, this process, referred to as lipotoxicity, can exacerbate skeletal muscle and liver sensitivity to insulin [6], pancreatic beta cell failure [7], and eventually chronic hyperglycemia [8].

Excess lipid accumulation, as observed in human obesity and T2D, results in numerous adaptations to the mitochondria, including reduced content [9], elevated production of reactive oxygen species (ROS) [10], increased mitochondrial fission [11], and blunted gene expression [12]. Furthermore, chronic nutrient oversupply to the mitochondria can cause incomplete fatty acid oxidation, leading to the accumulation of lipid byproducts and activation of pathways that drive insulin resistance [13, 14]. Peroxisome proliferator-activated receptor coactivator 1 alpha (PGC1α) is the main regulator of pathways that lead to mitochondrial biogenesis [15]. Its activation by AMP-activated protein kinase (AMPK) and silent information regulator 1 (SIRT1) promotes mitochondrial biogenesis and expression of numerous reactive oxygen species-detoxifying enzymes [16, 17].

Sphingolipids, including multiple ceramide species, have been shown to contribute to ectopic lipotoxicity [18, 19] and may interfere with cellular signaling pathways, thus promoting insulin resistance and type 2 diabetes. Elevated ceramide levels have been observed in both human obese and T2D patients [20–22], and pharmacologic inhibition in mice restored insulin sensitivity [23]. The aims of this experimental study were to assess changes in insulin sensitivity and regulatory mechanisms after surgically induced weight loss. Specifically, we hypothesized that RYGB would produce significant weight loss, increase PGC1α, SIRT1, AMPK, and citrate synthase (CS) protein expression and decrease insulin resistance, and these events would be associated with changes in levels of sphingolipids including ceramides and sphingosine-1-phosphate (S1P).

Materials and Methods

Animal Care and Surgery

Age-matched 12-14week-old homozygous recessive males (fa/fa) of the inbred Zucker diabetic fatty (ZDF) rat model were purchased from Charles River (Wilmington, MA). The animals were housed individually in controlled facilities (temperature 26°C ± 1°C, 40% humidity, 12 h light-dark cycle) with free access to water and a high carbohydrate diet (Purina 5008, Research Diet, New Brunswick, NJ). After a one-week quarantine period, the rats were randomly divided into two groups: RYGB surgery and sham surgery with 7 rats in each group. All experiments were approved by the Institutional Animal Care and Use Committee.

T2D was confirmed by the presence of hyperglycemia (> 250 mg/dL). Rats were fasted overnight and anesthetized with 2% isoflurane. Before surgery, ceftriaxone 75 mg/kg was administered intramuscularly for antimicrobial prophylaxis, and 10 ml of saline was given subcutaneously for hydration.

We used the gastric bypass model and bowel limb lengths as proposed by Meguid et al. [24] to achieve durable weight loss. A 4-cm upper midline incision was made. The stomach and distal esophagus were dissected free and a 20% proximal gastric pouch created. The jejunum was transected 30 cm distal to the ligament of Treitz, creating a 30-cm biliopancreatic limb. A 5-mm side-to-side gastrojejunostomy was made. A side-to-side jejuno-jejunal anastomosis was performed 10 cm below the gastrojejunostomy, creating a 10-cm alimentary limb. The abdomen was closed in layers. For the sham operation, the terminal esophagus and stomach were likewise exposed and dissected free. A 5-mm gastrotomy was made on the anterior surface of the gastric fundus and closed with interrupted sutures. The jejunum was also divided 30 cm below the ligament of Treitz and then reconnected. There was no surgical mortality in either group.

Pain was controlled with subcutaneous buprenorphine for the first 2 days postsurgery. The animals were provided an ad libitum liquid diet with Boost (Nestle, Buffalo Grove, IL) for 5 days after the surgery. For the remainder of the study, they were fed an ad libitum Purina 5008 diet. Body weight was measured weekly, and the gastrocnemius muscles were harvested at postoperative day 30.

Blood Sampling

Blood samples were collected at baseline and postoperative day 28 from the femoral vein, which was accessed using a cut-down technique. Blood samples were collected in EDTA tubes. After centrifugation, plasma was immediately separated and stored at − 80°C for subsequent measurements. Glucose was measured using the glucose oxidase assay (YSI Life Sciences, Yellow Springs, OH). Insulin was measured using

a multiplex kit (Millipore, Billerica, MA). Insulin resistance was estimated from fasting plasma glucose and insulin levels using the homeostasis model assessment of insulin resistance (HOMA-IR, fasting serum insulin (μU/ml) × fasting plasma glucose (mg/dl)/405) [25].

Immunoblotting

SIRT1, AMPK, phosphorylation of AMPK at the threonine 172 residue (pAMPK), PGC-1α, and CS protein expression were determined in white gastrocnemius muscle samples using a Western blot approach. Frozen muscle was homogenized with a glass homogenizer in freshly prepared phosphorprotein lysis buffer (cell extraction buffer, 10× of phosphatase-inhibitor cocktail, 0.3 M PMSF in DMSO, 10 ul of buffer per mg of muscle). The homogenate was incubated on ice for at least 30 min and centrifuged for 10 min at 12,000 rpm at 4 °C. Protein concentration was quantified using a commercial BCA protein assay kit (Pierce, Rockford, IL). A 20 μg protein extract was mixed with LDS sample buffer, and the protein was separated by 4–20% SDS-PAGE. After electrophoresis, the proteins were electrotransferred to a PVDF membrane (Bio-Rad, Hercules, CA). After blocking in PBST (5% instant nonfat dry milk, 0.1% Tween-20) for 1 h, the membranes were incubated overnight at 4 °C with primary antibody (1:1000 dilution) to either SIRT1, PGC-1α, AMPK, pAMPK (cell signaling), and citrate synthase (Alpha Diagnostics, San Antonio, TX). The membranes were washed 5 times for 5 min per each wash before incubation with secondary anti-rabbit IgG antibody (Diagnostic International, San Antonio, TX) for 1 h at room temperature. The membranes were washed with PBST again and subjected to enhanced chemiluminescence (Amersham Biosciences, Piscataway, NJ). The membranes were subsequently stripped with 0.5 M NaOH for 15 min at room temperature and reprobed with beta-actin primary antibody for 1 h at room temperature (Sigma, St Louis, MO). The membranes were washed several times with PBST before incubation with a secondary anti-mouse IgG antibody (Sigma, St Louis, MO). Membranes were developed using ECL prime reagent (GE Healthcare). The results were quantified by ImageJ, and changes in protein expression were normalized to beta-actin.

Tissues Ceramide Analysis

Ceramide species were quantified by high-performance liquid chromatography-mass spectrometry (LC-ESI-MS/MS). Frozen tissue samples were powdered under liquid nitrogen. For each analysis, an aliquot of tissue powder (7–15 mg wet weight) was suspended in ice-cold saline solution (500 μl, 1 M NaCl) and homogenized with a glass mortar and pestle. Calibration curves for ceramide standards using C17 and C25 ceramides as internal standards were prepared and processed in parallel with tissue samples. Ceramides from tissue homogenates were extracted using the protocol of Bligh and Dyer [26]. Briefly, 2 ml of an ice-cold chloroform, methanol (1:2, *v*/*v*) mixture was added to homogenized tissue and vortexed at 4°C. The pooled organic phase was filtered using a glass wool filter packed in a Pasteur pipette to remove any solid particles. The collected eluent was dried and the residue was reconstituted in HPLC elution buffer and analyzed by mass spectrometry. Ceramide species were quantified by HPLC online electrospray ionization tandem mass spectrometry (LC/ESI/MS/MS) [27]. Extracted samples (40 ul) were injected onto a Waters HPLC (2690 Separation Module, Waters, Corp., Franklin, MA) and separated through an Ascentis C18 column (2.1 × 50 mm, 5 um, SUPELCO, Bellefonte, PA) using a gradient starting from 15% mobile phase A (water containing 0.2% formic acid) at a flow rate of 0.3 ml/min, to 100% mobile phase B (acetonitrile/2-propanol (60:40.*v*/*v*) containing 0.2% formic acid) over 3 min, and then with 100% B for 22 min. The HPLC column effluent was introduced onto a micromass triple quadruple mass spectrometer (Quattro Ultima, Waters Inc., Beverly, MA) and analyzed using electrospray ionization in positive mode. All the tissue ceramides were quantified using multiple reaction monitoring. The MS/MS transitions (m/z) were 538→264 for C16:0, 552→264 for C17:0, 564→264 for C18:1, 566→264 for C18:0, 594→264 for C20:0, 622→264 for C22:0, 648→264 for C24:1, 650→264 for C24:0, and 664→264 for C25:0. Ceramide subspecies were quantified (nmol/ml) using calibration curves and the ratios of the integrated peak areas (MassLynx 3.5, Manchester, UK) of ceramide subspecies and internal standards. C17:0 ceramide was used as an internal standard for quantification of C16:0, C18:0, and C20:0 subspecies. Concentrations of C24:0 and C24:1 were quantified using C25:0 as an internal standard. Total measured ceramide was calculated from the sum of C16:0, C18:0, C18:1, C20:0, C22:0, C24:0, and C24:1 ceramide subspecies. All ceramide measurement experiments were normalized for wet tissue weight.

Tissue S1P Analysis

Tissue S1P was quantified by high-performance liquid chromatography-mass spectrometry (LC-ESI-MS/MS). Frozen tissue samples were powdered under liquid nitrogen. For each analysis, an aliquot of tissue powder (~25 mg wet weight) was suspended in ice-cold saline solution (500 μl, 1 M NaCl and 25 mM HCl) and homogenized with a glass mortar and pestle. Calibration curves for S1P standards using C17 S1P as internal standard were prepared and processed in parallel with tissue samples. Samples were ultrasonicated in ice-cold water for 1 min. Lipids were extracted by the addition of 0.5 ml of chloroform. The alkaline aqueous phase containing S1P was transferred to a glass tube and extracted twice

with a methanol/1 M NaCl (1:1 *v*/*v*) solution. The samples were dried in a speed vac overnight. The dried S1P residue was dissolved in 200 ul of methanol/water/acetic acid (50:50:1 v/v/v) and reconstituted in an LC-MS vial. All S1P measurements were normalized for wet tissue weight.

Statistical Analysis

Data are presented as mean ± standard error (SE). All statistical analyses were performed using GraphPad Prism version 7.0 (GraphPad Software, La Jolla, CA). Comparisons between RYGB and sham control for the ceramide sub-species was performed via two-way analysis of variance (ANOVA) with Sidak's multiple comparisons test. All other comparisons between groups were assessed using an unpaired Student's *t* test. If unequal variance between groups existed, the *t* test was adjusted using Welch's correction. Associations between study variables were determined using Pearson's *r*. In all tests, $P < 0.05$ was considered statistically significant.

Results

Baseline characteristics including body weight, fasting glucose, and insulin were similar between study groups. At 28 days postoperatively, the animals who undergone RYGB had significantly lower body weight ($P < 0.01$), fasting plasma glucose ($P < 0.05$), insulin ($P < 0.001$), triglycerides ($P < 0.05$), and HOMA ($P < 0.001$) compared with the sham group (Table 1).

Tissue expression of AMPK, pAMPK, SIRT1, PGC-1α, and CS was significantly increased in RYGB compared with the sham group (Fig. 1a–d). The concentration of ceramides, S1P, and the distribution of ceramide subspecies in skeletal muscles of ZDF rats are illustrated in Fig. 2. RYGB significantly reduced C18:0 ($P = 0.001$), whereas C16:0, C18:1, C20:0, C22:0, C24:0, and C24:1 remained unchanged (Fig. 2a). Additionally, there was a reduction in total ceramides ($P = 0.09$) and the ratio of total ceramides to S1P ($P < 0.05$) (Fig. 2b and c). The concentration of S1P was significantly increased ($P < 0.01$) after RYGB compared with sham controls (Fig. 2d).

In order to better determine potential relationships between the ratio of total tissue ceramide and S1P levels with weight change, the degree of insulin resistance, and the level of expression of SIRT1, PGC1-α, and citrate synthase, correlations were assessed using Pearson's *r*. Twenty-eight days after surgery, the ceramide/S1P ratio correlated with weight loss ($r = 0.50$, $P = 0.06$, Fig. 3a), such that rats with the greatest weight loss also had the greatest decrease in ratio. The decrease in ceramide/S1P ratio was also positively correlated with a decrease in insulin resistance as measured by HOMA ($r = 0.61$, $P = 0.02$, Fig. 3b) and an increase in SIRT1 ($r = -0.54$, $P = 0.04$, Fig. 3c), PGC1-1α ($r = -0.51$, $P = 0.06$, Fig. 3d), and citrate synthase ($r = -0.63$, $P = 0.01$, Fig. 3e) protein expression.

Table 1 Characteristics of sham and RYGB mice 28 days after surgery

	Sham ($N = 7$)	RYGB ($N = 7$)
Age (weeks)	17 ± 1.0	17 ± 1.0
Body weight (g)	397.9 ± 19.2	281.8 ± 19.7**
Glucose (mg/dL)	275.6 ± 23.5	213.8 ± 16.1*
Insulin (pM)	278.8 ± 16.0	48.3 ± 7.0***
Triglycerides (mg/dL)	29.5 ± 2.4	17.7 ± 2.9*
HOMA	27.5 ± 2.6	3.8 ± 1.0***

Values are presented as mean ± SE. *$P < 0.05$, **$P < 0.01$, ***$P < 0.001$ vs. sham

Discussion

Bariatric surgery is the most effective long-term treatment for obesity and offers the greatest chance for improvement and resolution of obesity-related comorbidities. In the current study, we investigated cellular changes in proteins that have been implicated in insulin resistance and type 2 diabetes, using an obese diabetic rat model and RYGB surgery. We found that RYGB markedly increased AMPK, SIRT1, PGC-1α, citrate synthase, and S1P expression while reducing ceramide activity. Additionally, we observed that the ratio of ceramide to S1P was decreased after RYGB, and these changes negatively correlated with metabolic improvements and cellular adaptations after surgically induced weight loss. We therefore postulate that a central adaptive mechanism to RYGB is upregulation of energy sensing pathways, which then coordinate improvements in substrate utilization, lipid trafficking, and peripheral insulin sensitivity.

Insulin resistance is a principal defect underlying obesity-induced T2D. Lipid accumulation in skeletal muscle and other insulin targeted tissues, including the liver, damages the insulin-signaling cascade and promotes insulin resistance, a pathologic event that is called lipotoxicity [28–32]. Among the different types of lipids involved in lipotoxicity, it is well documented in animal and human studies that ectopic accumulation of ceramides in the liver and skeletal muscle inhibits insulin action and subsequent glucose uptake through inactivation of Akt [33]. We have previously shown that plasma ceramides are elevated in obese patients with T2D and the high levels correlate with insulin resistance and inflammation [20]. In addition, reduction in insulin resistance after bariatric surgery is associated with a significant reduction in plasma [11] and urinary ceramide levels [19]. The results of the current study parallel previous data and show that total ceramide and subspecies in skeletal muscle decrease after RYGB, and

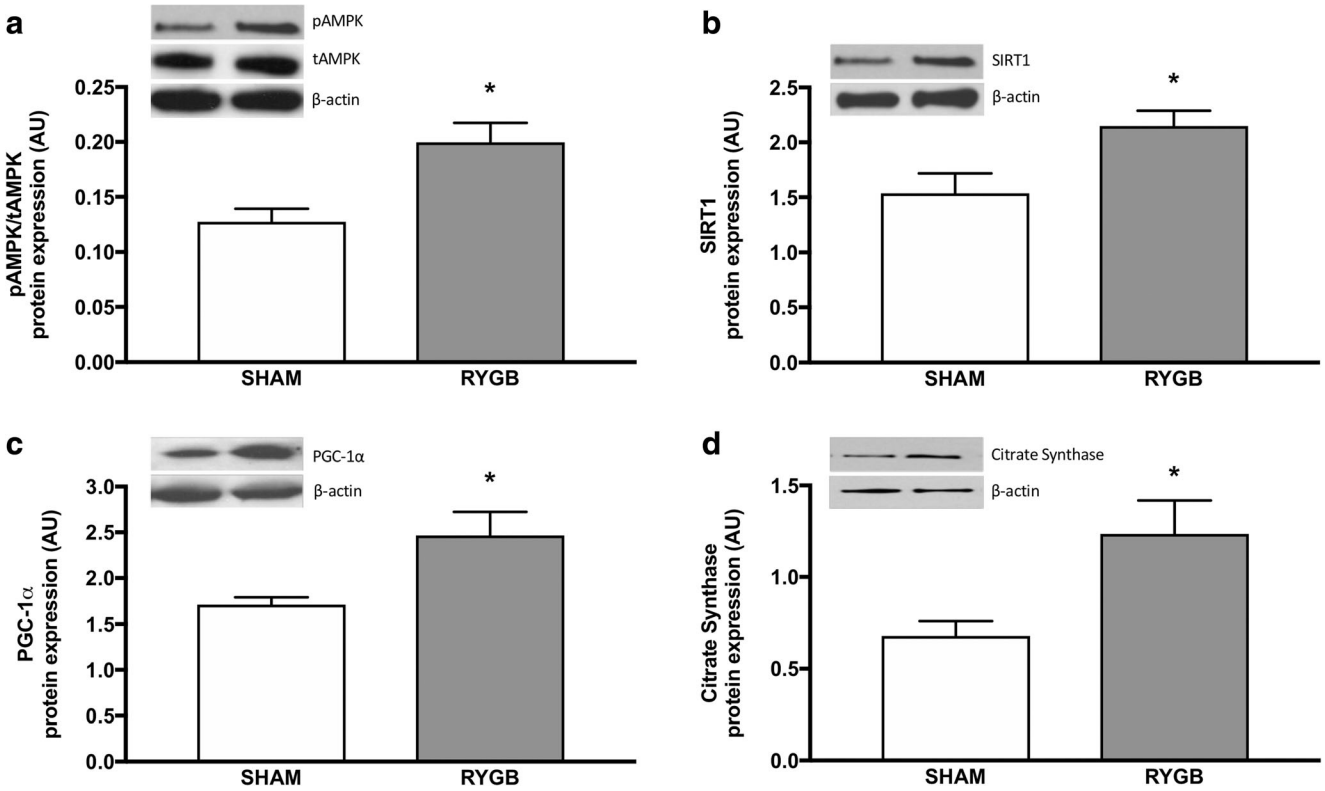

Fig. 1 Changes in AMPK phosphorylation (**a**), SIRT1 (**b**), PGC-1α (**c**) and citrate synthase (**d**) expression in white gastrocnemius skeletal muscle after RYGB compared with sham control. Representative Western blots are shown above the graphs. Values are expressed as means ± SE. * $P < 0.05$ RYGB vs. sham

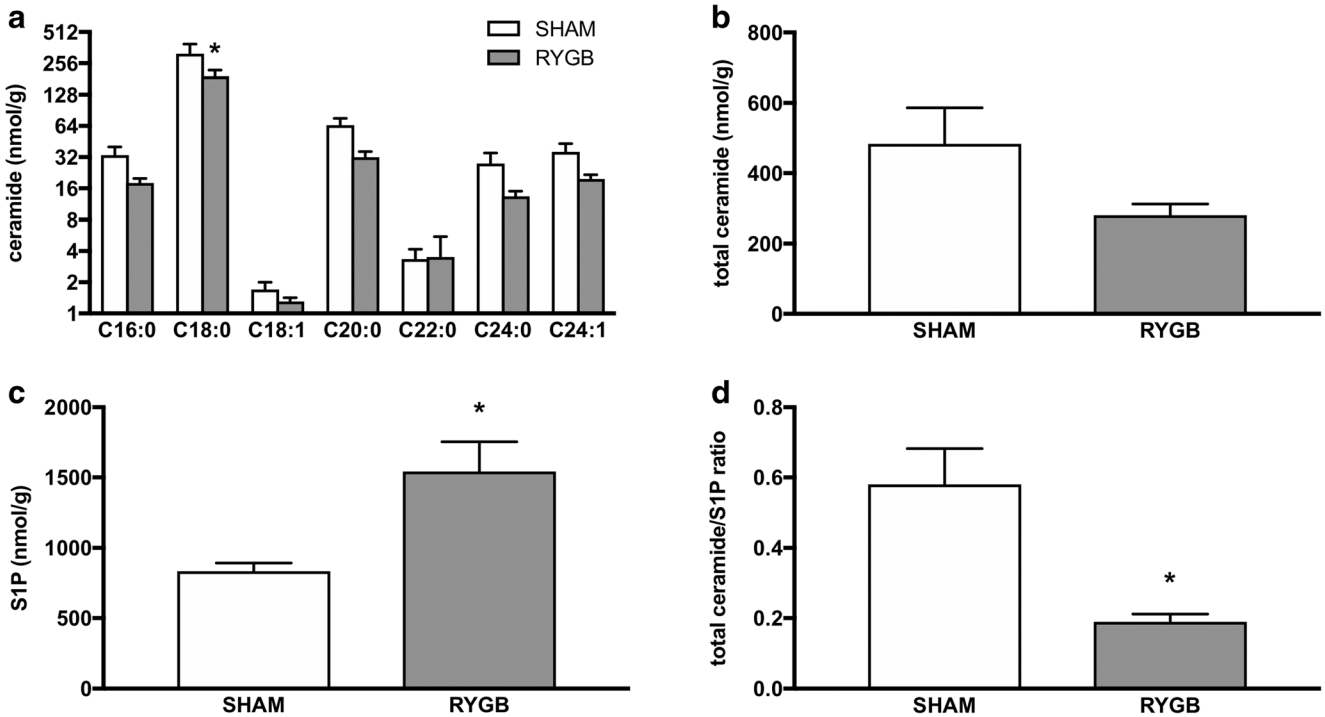

Fig. 2 Changes in skeletal muscle ceramide species (**a**), total ceramides (**b**), and S1P concentrations (**c**), as well as the ratio of total ceramides to S1P (**d**) after RYGB compared with sham. Values are expressed as means ± SE. * $P < 0.05$ RYGB vs. sham control

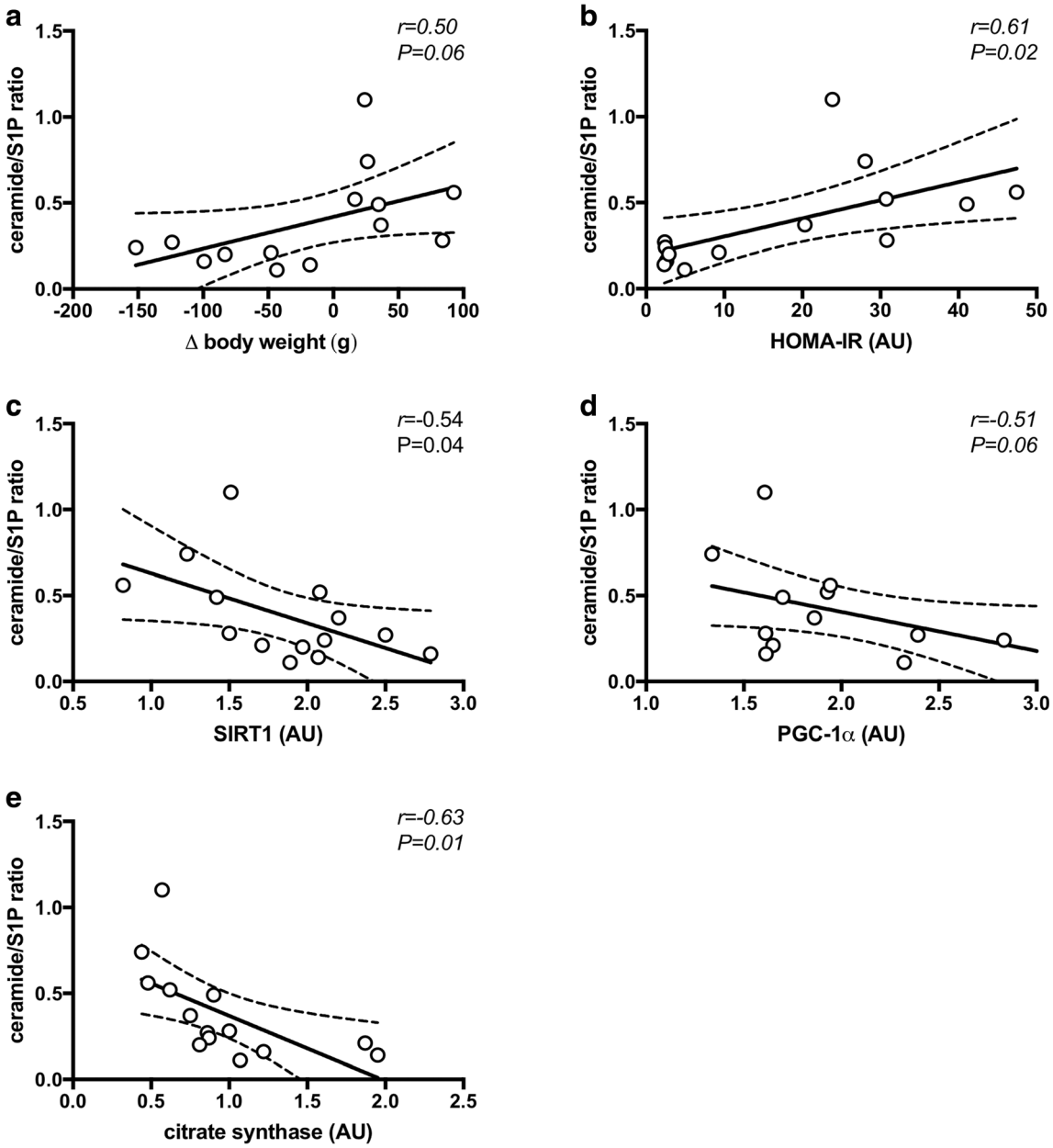

Fig. 3 Correlations between the ratio of total ceramides to S1P and metabolic parameters after surgery in RYGB and sham control. Decreased ratio of total ceramides to S1P was positively correlated with change in body weight ($r = 0.50$, $P = 0.06$) (**a**) and HOMA-IR ($r = 0.61$, $P = 0.02$) (**b**) and negatively correlated with SIRT1 ($r = -0.54$, $P = 0.04$) (**c**), PGC-1α ($r = -0.51$, P = 0.06) (**d**), and citrate synthase ($r = -0.63$, $P = 0.01$) expression (**e**)

these changes are positively correlated with changes in body weight and HOMA-IR.

S1P is a sphingolipid with important structural and functional roles in cell signaling, proliferation, differentiation, survival, and apoptosis [34, 35]. Early studies identified increased levels of S1P in human and rodent models of obesity [36, 37]. In this view, S1P production occurs as a result of increased free fatty acids and can drive comorbidities associated with obesity and T2D, such as atherosclerosis, and hypertension [38, 39]. However, mice treated with a synthetic analog of S1P, FTY720, were protected against diet-induced obesity [40]. Additionally, FTY720-treated animals displayed increased adipose tissue AMPK phosphorylation, similar to the results described herein. Inhibition of S1P in pancreatic beta cells impairs glucose-stimulated insulin secretion, further supporting the metabolic role of sphingolipids [41]. Under nonpathologic conditions, S1P is readily absorbed in the gastrointestinal tract [42]. Weight loss following RYGB is achieved through both nutrient restriction, achieved by the creation of a small gastric pouch, and malabsorption by alternation of the jejunal anatomy [43]. Therefore, one may speculate that S1P-mediated metabolic improvements after RYGB

result from impaired lipid degradation, subsequently increasing uptake by peripheral tissues, and inhibiting endogenous synthesis.

Mitochondrial content and biogenesis are reduced in obesity and T2D. Reduced content in the presence of nutrient oversupply can overload the mitochondria, resulting in impaired oxidation, accumulation of intracellular lipids, and insulin resistance. Expression of PGC1α, a transcriptional regulator of mitochondrial biogenesis, is reduced in obese and T2D's [12, 44]. In the current study, RYGB reduced insulin resistance and enhanced skeletal muscle protein expression in the AMPK-SIRT1-PGC-1α pathway. We have previously demonstrated that RYGB results in chronic upregulation in hepatic citrate synthase activity and PGC-1α expression [45]. Others have shown in vitro that increased PGC-1α expression induces insulin signaling via the upregulation of specific genes involved in fatty acid beta-oxidation, glucose transport, and oxidative phosphorylation [46, 47]. Phosphorylation by AMPK and deacetylation by SIRT1 are two pathways that activate PGC-1α which result in mitochondrial biogenesis.

AMPK is considered a key regulator of fat and carbohydrate metabolism [17], and its activation enhances pathways that generate ATP, such as phosphorylation and activation of PGC-1α, glucose transport and fatty acid oxidation, and inhibits ATP-consuming pathways including triglycerides and cholesterol synthesis. New therapies designed to increase AMPK have been examined in the treatment of insulin resistance, T2D, and associated metabolic disorders [17, 48–51]. SIRT1 is the main deacetylase of PGC-1α, and it is known to positively regulate mitochondrial and fatty acid utilization genes [16]. Furthermore, SIRT1 increases lipolytic rates in white adipose tissue [52] and insulin secretion in beta cells of the pancreas [53]. In a rat model, RYGB surgery has been shown to upregulate AMPK and SIRT1 signaling pathways [41]. However, since we did not have a pair-fed group weight matched to the RYGB group, it was not possible to determine whether the mechanisms responsible for the metabolic improvements following RYGB were weight loss dependent.

In conclusion, the results of this study indicate that RYGB reduces insulin resistance and skeletal muscle ceramide accumulation. This occurred in conjunction with a significant increase in skeletal muscle S1P and activation of AMPK-SIRT1-PGC1α pathways. Further mechanistic and clinical research is needed to better delineate the cellular and molecular mechanisms responsible for reductions in lipotoxicity and insulin resistance following bariatric surgery.

Funding Information This research was supported by the American Society of Metabolic and Bariatric Surgery, the National Institute of Diabetes and Digestive and Kidney Diseases (DK108089), internal funding from the Cleveland Clinic Research Program Committee (#2010-1009), and the Louisiana Clinical and Translational Science Center (U54 GM104940).

Compliance with Ethical Standards

All experiments were approved by the Institutional Animal Care and Use Committee.

Conflict of Interest The authors declare that they have no conflict of interest.

Ethics Approval Statement All applicable institutional and/or national guidelines for the care and use of animals were followed. This article does not contain any studies with human participants performed by the authors.

Publisher's Note Springer Nature remains neutral with regard to jurisdictional claims in published maps and institutional affiliations.

References

1. Buchwald H, Estok R, Fahrbach K, et al. Weight and type 2 diabetes after bariatric surgery: systematic review and meta-analysis. Am J Med. 2009;122(3):248–56. e5
2. Brethauer SA et al. Can diabetes be surgically cured? Long-term metabolic effects of bariatric surgery in obese patients with type 2 diabetes mellitus. Ann Surg. 2013;258(4):628–36. discussion 636-7
3. Schauer PR, Bhatt DL, Kirwan JP, et al. Bariatric surgery versus intensive medical therapy for diabetes - 5-year outcomes. N Engl J Med. 2017;376(7):641–51.
4. Abu-Gazala S, Horwitz E, Ben-Haroush Schyr R, et al. Sleeve gastrectomy improves glycemia independent of weight loss by restoring hepatic insulin sensitivity. Diabetes. 2018;67(6):1079–85.
5. Bramante CT, Lee CJ, Gudzune KA. Treatment of obesity in patients with diabetes. Diabetes Spectr. 2017;30(4):237–43.
6. Bonnard C, Durand A, Peyrol S, et al. Mitochondrial dysfunction results from oxidative stress in the skeletal muscle of diet-induced insulin-resistant mice. J Clin Invest. 2008;118(2):789–800.
7. Lee Y, Hirose H, Ohneda M, et al. Beta-cell lipotoxicity in the pathogenesis of non-insulin-dependent diabetes mellitus of obese rats: impairment in adipocyte-beta-cell relationships. Proc Natl Acad Sci U S A. 1994;91(23):10878–82.
8. Itani SI, Ruderman NB, Schmieder F, et al. Lipid-induced insulin resistance in human muscle is associated with changes in diacylglycerol, protein kinase C, and IkappaB-alpha. Diabetes. 2002;51(7):2005–11.
9. Kelley DE, He J, Menshikova EV, et al. Dysfunction of mitochondria in human skeletal muscle in type 2 diabetes. Diabetes. 2002;51(10):2944–50.
10. Anderson EJ, Lustig ME, Boyle KE, et al. Mitochondrial H2O2 emission and cellular redox state link excess fat intake to insulin resistance in both rodents and humans. J Clin Invest. 2009;119(3):573–81.
11. Jheng HF, Tsai PJ, Guo SM, et al. Mitochondrial fission contributes to mitochondrial dysfunction and insulin resistance in skeletal muscle. Mol Cell Biol. 2012;32(2):309–19.
12. Mootha VK, Lindgren CM, Eriksson KF, et al. PGC-1alpha-responsive genes involved in oxidative phosphorylation are coordinately downregulated in human diabetes. Nat Genet. 2003;34(3):267–73.
13. Wensaas AJ, Rustan AC, Just M, et al. Fatty acid incubation of myotubes from humans with type 2 diabetes leads to enhanced release of beta-oxidation products because of impaired fatty acid oxidation: effects of tetradecylthioacetic acid and eicosapentaenoic acid. Diabetes. 2009;58(3):527–35.

14. Adams SH, Hoppel CL, Lok KH, et al. Plasma acylcarnitine profiles suggest incomplete long-chain fatty acid beta-oxidation and altered tricarboxylic acid cycle activity in type 2 diabetic African-American women. J Nutr. 2009;139(6):1073–81.
15. Lin J, Handschin C, Spiegelman BM. Metabolic control through the PGC-1 family of transcription coactivators. Cell Metab. 2005;1(6):361–70.
16. Gerhart-Hines Z, Rodgers JT, Bare O, et al. Metabolic control of muscle mitochondrial function and fatty acid oxidation through SIRT1/PGC-1alpha. EMBO J. 2007;26(7):1913–23.
17. Canto C, Auwerx J. PGC-1alpha, SIRT1 and AMPK, an energy sensing network that controls energy expenditure. Curr Opin Lipidol. 2009;20(2):98–105.
18. Zhou YT, Grayburn P, Karim A, et al. Lipotoxic heart disease in obese rats: implications for human obesity. Proc Natl Acad Sci U S A. 2000;97(4):1784–9.
19. Huang H, Kasumov T, Gatmaitan P, et al. Gastric bypass surgery reduces plasma ceramide subspecies and improves insulin sensitivity in severely obese patients. Obesity (Silver Spring). 2011;19(11):2235–40.
20. Haus JM, Kashyap SR, Kasumov T, et al. Plasma ceramides are elevated in obese subjects with type 2 diabetes and correlate with the severity of insulin resistance. Diabetes. 2009;58(2):337–43.
21. Adams 2nd JM et al. Ceramide content is increased in skeletal muscle from obese insulin-resistant humans. Diabetes. 2004;53(1):25–31.
22. Broskey NT, Obanda DN, Burton JH, et al. Skeletal muscle ceramides and daily fat oxidation in obesity and diabetes. Metabolism. 2018;82:118–23.
23. Holland WL, Brozinick JT, Wang LP, et al. Inhibition of ceramide synthesis ameliorates glucocorticoid- , saturated-fat- , and obesity-induced insulin resistance. Cell Metab. 2007;5(3):167–79.
24. Meguid MM, Ramos EJ, Suzuki S, et al. A surgical rat model of human Roux-en-Y gastric bypass. J Gastrointest Surg. 2004;8(5):621–30.
25. Matthews DR, Hosker JP, Rudenski AS, et al. Homeostasis model assessment: insulin resistance and beta-cell function from fasting plasma glucose and insulin concentrations in man. Diabetologia. 1985;28(7):412–9.
26. Bligh EG, Dyer WJ. A rapid method of total lipid extraction and purification. Can J Biochem Physiol. 1959;37(8):911–7.
27. Kasumov T, Huang H, Chung YM, et al. Quantification of ceramide species in biological samples by liquid chromatography electrospray ionization tandem mass spectrometry. Anal Biochem. 2010;401(1):154–61.
28. Benton CR, Nickerson JG, Lally J, et al. Modest PGC-1alpha overexpression in muscle in vivo is sufficient to increase insulin sensitivity and palmitate oxidation in subsarcolemmal, not intermyofibrillar, mitochondria. J Biol Chem. 2008;283(7):4228–40.
29. Bruce CR, Hoy AJ, Turner N, et al. Overexpression of carnitine palmitoyltransferase-1 in skeletal muscle is sufficient to enhance fatty acid oxidation and improve high-fat diet-induced insulin resistance. Diabetes. 2009;58(3):550–8.
30. Hill JO et al. Obesity and the environment: where do we go from here? Science. 2003;299(5608):853–5.
31. Holland WL, Knotts TA, Chavez JA, et al. Lipid mediators of insulin resistance. Nutr Rev. 2007;65(6 Pt 2):S39–46.
32. Houmard JA. Intramuscular lipid oxidation and obesity. Am J Physiol Regul Integr Comp Physiol. 2008;294(4):R1111–6.
33. Arboleda G, Cárdenas Y, Rodríguez Y, et al. Differential regulation of AKT, MAPK and GSK3beta during C2-ceramide-induced neuronal death. Neurotoxicology. 2010;31(6):687–93.
34. Cuvillier O, Pirianov G, Kleuser B, et al. Suppression of ceramide-mediated programmed cell death by sphingosine-1-phosphate. Nature. 1996;381(6585):800–3.
35. Taha TA, Kitatani K, el-Alwani M, et al. Loss of sphingosine kinase-1 activates the intrinsic pathway of programmed cell death: modulation of sphingolipid levels and the induction of apoptosis. FASEB J. 2006;20(3):482–4.
36. Ito S, Iwaki S, Koike K, et al. Increased plasma sphingosine-1-phosphate in obese individuals and its capacity to increase the expression of plasminogen activator inhibitor-1 in adipocytes. Coron Artery Dis. 2013;24(8):642–50.
37. Kowalski GM, Carey AL, Selathurai A, et al. Plasma sphingosine-1-phosphate is elevated in obesity. PLoS One. 2013;8(9):e72449.
38. Cantalupo A, Di Lorenzo A. S1P signaling and de novo biosynthesis in blood pressure homeostasis. J Pharmacol Exp Ther. 2016;358(2):359–70.
39. Keul P, Lucke S, von Wnuck Lipinski K, et al. Sphingosine-1-phosphate receptor 3 promotes recruitment of monocyte/macrophages in inflammation and atherosclerosis. Circ Res. 2011;108(3):314–23.
40. Moon MH, Jeong JK, Lee JH, et al. Antiobesity activity of a sphingosine 1-phosphate analogue FTY720 observed in adipocytes and obese mouse model. Exp Mol Med. 2012;44(10):603–14.
41. Cantrell Stanford J, Morris AJ, Sunkara M, et al. Sphingosine 1-phosphate (S1P) regulates glucose-stimulated insulin secretion in pancreatic beta cells. J Biol Chem. 2012;287(16):13457–64.
42. Kihara A, Mitsutake S, Mizutani Y, et al. Metabolism and biological functions of two phosphorylated sphingolipids, sphingosine 1-phosphate and ceramide 1-phosphate. Prog Lipid Res. 2007;46(2):126–44.
43. Sawaya RA et al. Vitamin, mineral, and drug absorption following bariatric surgery. Curr Drug Metab. 2012;13(9):1345–55.
44. Patti ME, Butte AJ, Crunkhorn S, et al. Coordinated reduction of genes of oxidative metabolism in humans with insulin resistance and diabetes: potential role of PGC1 and NRF1. Proc Natl Acad Sci U S A. 2003;100(14):8466–71.
45. Sacks J et al. *Effect of Roux-en-Y gastric bypass on liver mitochondrial dynamics in a rat model of obesity*. Physiol Rep. 2018:**6**(4).
46. Koves TR, Li P, An J, et al. Peroxisome proliferator-activated receptor-gamma co-activator 1alpha-mediated metabolic remodeling of skeletal myocytes mimics exercise training and reverses lipid-induced mitochondrial inefficiency. J Biol Chem. 2005;280(39):33588–98.
47. Michael LF, Wu Z, Cheatham RB, et al. Restoration of insulin-sensitive glucose transporter (GLUT4) gene expression in muscle cells by the transcriptional coactivator PGC-1. Proc Natl Acad Sci U S A. 2001;98(7):3820–5.
48. Musi N, Fujii N, Hirshman MF, et al. AMP-activated protein kinase (AMPK) is activated in muscle of subjects with type 2 diabetes during exercise. Diabetes. 2001;50(5):921–7.
49. Winder WW. AMP-activated protein kinase: possible target for treatment of type 2 diabetes. Diabetes Technol Ther. 2000;2(3):441–8.
50. Winder WW, Hardie DG. AMP-activated protein kinase, a metabolic master switch: possible roles in type 2 diabetes. Am J Phys. 1999;277(1 Pt 1):E1–10.
51. Witczak CA, Sharoff CG, Goodyear LJ. AMP-activated protein kinase in skeletal muscle: from structure and localization to its role as a master regulator of cellular metabolism. Cell Mol Life Sci. 2008;65(23):3737–55.
52. Picard F, Kurtev M, Chung N, et al. Sirt1 promotes fat mobilization in white adipocytes by repressing PPAR-gamma. Nature. 2004;429(6993):771–6.
53. Bordone L, Motta MC, Picard F, et al. Sirt1 regulates insulin secretion by repressing UCP2 in pancreatic beta cells. PLoS Biol. 2006;4(2):e31.